RSC Advances

ROYAL SOCIETY OF CHEMISTRY

www.rsc.org/advances

RSC Advances

ARTICLE

Furthering the Chemosensing of Silver Nanoclusters for Ions Detection

Received 00th January 20xx,
Accepted 00th January 20xx

DOI: 10.1039/x0xx00000x

www.rsc.org/

Weihua Ding,[a,b] Saipeng Huang,[a,b] Lingmei Guan,[a,b] Xianhu Liu,[a,b] Zhixun Luo*[a]

Ligand-protected metal nanoclusters (NCs) having hydrodynamic diameters and fluorescent properties bear reasonable potentials for ions detection and bio-imaging applications by taking advantages of smaller sizes and degradability comparing with large nanoparticles (NPs). By controlling the pH-value, here we have synthesized a fluorescent silver nanocluster — Ag-glutathione, which is found a versatile chemosensor operative for the detection of both manganese (Mn^{2+}) and iodine (I^-) ions. Mn^{2+} and I^- are further distinguished by the ratiometric absorption spectrometry method. Care was taken for the sufficient spectral analyses upon which we have fully demonstrated the chemosensing mechanisms of Ag@SG NCs (Ag@glutathione nanoclusters) applied in ions detection. Having expounded this issue, we further excavated the potential application of Ag@SG NCs in bioimaging. It is interesting to find that the as-prepared Ag@SG NCs are nontoxic avaliable for fluorescence imaging of MCF-7 cells, with on/off alternation of fluorescence emission at the presence of Mn^{2+} or I^- ions. The low cytotoxicity, good penetrability and fluorescence on/off property of Ag@SG NCs in MCF-7 cells suggest promising biological applications.

1. Introduction

Detection of cationic and anionic ions is important in industrial wastes and environmental processes, where the specific ion determination helps monitor excessive or deficient levels in soils and water.[1, 2] Overmuch ions existing in natural water and plants due to contamination of ground water, surface water and soils can enter human body through foods and drinking water resulting in poisoning, which has been a serious concern in many areas of the globe. It is still notable that necessary trace elements (e.g. Cu^{2+}, Mn^{2+}, Fe^{3+}, Zn^{2+}, I^-, and other ions) are essentially involved in diverse fundamental biological processes, and a small amount of these necessary trace elements plays an important role in biological activities, however the presence of large amounts in human body may lead to severe health issues. Thus it becomes important to develop effective methods for ions detection not only in soils and drinking water, but also in body and living cells.

On this purpose extensive strategies have been used in the past, including chromatography, electrochemical analysis, spectrometry by artificial chromophore and fluorophore, etc.[3] Among these available detection methods, fluorescence chemosensors such as conjugated fluorescent polymer stimulated increasing research interest owing to their high sensitivity and simplicity with rapid response.[4] Recently, with development of nanotechnology, nanoscaled fluorescent chemosensors have become the mostly applied analytical methods to detect and trace ions in aqueous solution.[5-9] It has been recognized that metal nanoclusters (NCs, c.a., small nanoparticles having sizes between 1 and 10 nanometers) encapsulated in different scaffolds such as thiols and even DNA, etc., are operative for ions detection as the ligand protection provides enhanced stability frequently under a superatom cluster concept.[10-13] Blooming advances in this field enable promising future to design NCs-based chemosensors promulgated with notable optical, electrical and chemical properties for bioimaging and ions detection.[14-26]

However, a common view in this field is that chemosensors are usually valid either for detection of a cationic ion or an anionic ion, thus a pending question remains that what happens if both cationic and anionic ions coexist in a complex unknown solution. Also, rare fluorescent chemosensors have been applied in living cells by far to our best knowledge. It is highly desirable to develop eco-friendly and nontoxic fluorescent chemosensors with high sensitivity for ions detection. Facile synthesis procedure and high selective capability are expected in order to enable detection of multiple ions simultaneously. In addition, the predominant sensing mechanism varies depending on the type of the sensor, and is abided strictly by the altering of fluorescence property of the NCs through specific

[a] State Key Laboratory for Structural Chemistry of Unstable and Stable Species, Institute of Chemistry, Chinese Academy of Sciences, Beijing 100190, P. R. China. E-mail: zxluo@iccas.ac.cn
[b] Graduate University of Chinese Academy of Sciences (GUCAS), Beijing 100049, P. R. China.

† Electronic Supplementary Information (ESI) available: [Chemicals, properties of the silver clusters, more spectral experimental details]. See DOI: 10.1039/b000000x/.

interactions with either the metallic core or the protecting ligand.[27-31] These issues are still illusive to be further explored.

Thanks to the biocompatible glutathione (HSG) which doesn't exhibit cytotoxicity itself, and Ag-glutathione complex also doesn't show obvious cytotoxicity with the concentrations up to mmol/L.[2, 32-36] Motivated on this, here we have synthesized eco-friendly silver NCs, and performed an indepth study of ions detection utilizing the Ag@SG NCs as fluorescence chemosensor. It is interesting to find that the as-prepared Ag NCs chemosensor is operative for the detection and differentiation of Mn^{2+} and I^- ions. Together with an insight into the sensing mechanisms, we demonstrate feasible applications in living cells with on/off controllability at the presence of predetermined ions.

2. Experimental

2.1 Materials and Synthesis

All chemicals were commercially available and used as received without further purification.

The glutathione-protected silver nanoclusters (Ag@SG NCs for short) were synthesized according to the following procedure (**Scheme 1**). Firstly, the aqueous solution of $AgNO_3$ (84.9 mg, 0.5 mM) and glutathione (GSH; 615.0 mg, 2.0 mM) were mixed together in 25 mL water with vigorous stirring, and the solution was kept at ~0°C in an ice bath. Next, an aqueous solution of NaOH (0.5 M) was added into the above solution until the white precipitate completely disappeared (PH=6). To this clear solution, a freshly prepared ice-cold aqueous $NaBH_4$ (189.0 mg, 5.0 mL) were slowly added dropwise under vigorous stirring condition. Then, the reaction was allowed to proceed under constant stirring for 7 h, and the clusters were precipitated with methanol. After filtration, brown precipitate of Ag@SG NCs was obtained, and then washed with excessive methanol.

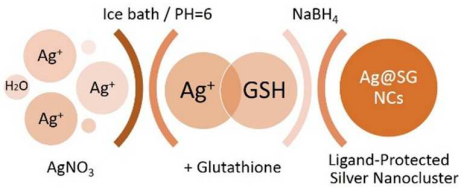

Scheme 1. A sketch drawing depicting the synthesis procedure of glutathione-protected silver nanoclusters in this study.

2.2 Measurements and Characterization

Fluorescence spectra were collected on a Horiba Scientific Fluoromax-4 spectrophotometer equipped with a quartz cuvette of 1.0 cm path length with a xenon lamp as the excitation source. UV-Vis absorption spectra were recorded on a UV-3600 spectrophotometer. Fourier transform infrared (FT-IR) spectra were obtained on an Avatar 360 FI-IR spectrometer in the range of 4000–400 cm^{-1}. The ^1H NMR spectra were measured on a Bruker Avance III 400 MH_Z spectrometer in D_2O solution with TMS as an internal standard. Transmission electron microscopy (TEM) images were captured with a JEOL JEM-2100F field-emission transmission electron microscopy with an accelerating voltage at 200 kV. X-ray photoelectron spectroscopy (XPS) was performed on the Thermo Scientific ESCALab 250Xi. Mass spectra were determined with a Bruker Solarix 9.4 T high resolution mass spectrometer by using an electron spray ion source.

Ions detections were conducted in a quartz cuvette (1 cm beam path). Briefly, small amounts of concentrated salt solutions were added to the Ag@SG NCs water solution, which did not give rise to obvious pH value changes. In all titration experiments, the metal cations (Fe^{3+}, Co^{2+}, Cd^{2+}, Ca^{2+}, Cr^{3+}, Cu^{2+}, Pb^{2+}, Ni^{2+}, Zn^{2+} and Mn^{2+}) and anions (F^-, Cl^-, Br^-, I^-, NO_2^-, CO_3^{2-}, AcO^-, $H_2PO_4^-$, HCO_3^-, SO_4^{2-}, HPO_4^{2-}, HSO_3^-, and OH^-) were refereed to normal ionic compounds as largely used in this field.[37-41]

The *in vitro* cytotoxicity was measured using the methyl thiazolyl tetrazolium (MTT) assay in MCF-7 cell lines. Cells in log-growth phase were seeded into a 96-well cell-culture plate at 1×10^4 per well in 100 µL DMEM (Dulbecco's Modified Eagle Medium). Ag@SG NCs were added to the wells (100 µL/well) of the treatment group, and the final concentration was ranged from 0 to 0.5 µg/mL. The cells were incubated for 24 h at 37 °C under 5% CO_2. The combined MTT/PBS solution (100 µL, 0.5 mg/mL) was added to each well of the 96-well assay plate, and incubated for an additional 2 h. An enzyme-linked immunosorbent assay (ELISA) reader (µQuant, Bio-Tek, USA) was used to measure the OD570 (Absorbance value) of each well referenced at 690 nm. The formula used to calculate the viability of cell growth is: Viability (%) = (the mean absorbance value of treatment group/mean absorbance value of control) ×100.

Prior to the bioimaging experiment, MCF-7 cells were cultured in DMEM. Cells were incubated with 0.25 µg/mL Ag@SG NCs at 37 °C for 2 h. After washing with PBS three times to remove remaining Ag@SG NCs, the cells were then incubated with proper concentration of Mn^{2+} and I^- solution for 30 min at room temperature, respectively. The incubated cells were washed with PBS and mounted onto a glass slide. Fluorescence images of the mounted cells were obtained using a confocal laser scanning microscope at 488-nm excitation.

3. Results and Discussion

3.1 Detecting both Mn^{2+} and I^- ions

Fig. 1a presents an UV–Vis absorption spectrum of the as-prepared Ag@SG NCs, where a broad absorption band from 350 nm to 500 nm is noted largely differing from the plasmon resonance absorption spectrum of large silver nanoparticles (c.a., >10nm) which bear a narrow peak at about ~400nm wave length. We checked the sizes of the obtained Ag@SG NCs by TEM photography and found that they are spherical, well dispersed with an average size of ~3 nm, as shown by the two inset images. (More details in **Fig. 1a,** and **Fig S1a, ESI**).

The Ag@SG NCs exhibit an intense fluorescence emission package centred at ~630 nm (**Fig. 1b,** excited at 400 nm). As a comparison, also provided is the excitation spectrum which is consistent with the aforementioned UV-Vis absorption behaviour. In addition, the mono-dispersity of the Ag@SG NCs product was checked by polyacrylamide gel electrophoresis (PAGE) analysis (**Fig.**

S1b, **ESI**), which indicates decent grade of purity of the as-prepared clusters. XPS (**Fig. S3a and 3b, ESI**) survey spectrum of the Ag@SG NCs confirms the presence of Ag, S, C, N, O elements, and the Ag $3d_{5/2}$ peak at 368.2 eV is close to an Ag(0) value, which matches the previously published report;[42] the presence of S ($2p_{3/2}$) at 162.3 eV suggests that the ligand is chemically bonded to silver cluster in the form of thiolates,[43] which is in agreement with the IR spectrum (**Fig. S4**, **ESI**) where the 2523 cm^{-1} mode belonging to the S-H stretching of a HSG molecule disappears, evidencing that the formation of Ag@SG NCs is stabilized by S-Ag bindings.[42] In addition, the auger electron peak of silver (**Fig. S3c, ESI**) confirms the presence of Ag(I); in other words, Ag(0) and Ag(I) coexisted in Ag@SG NCs.

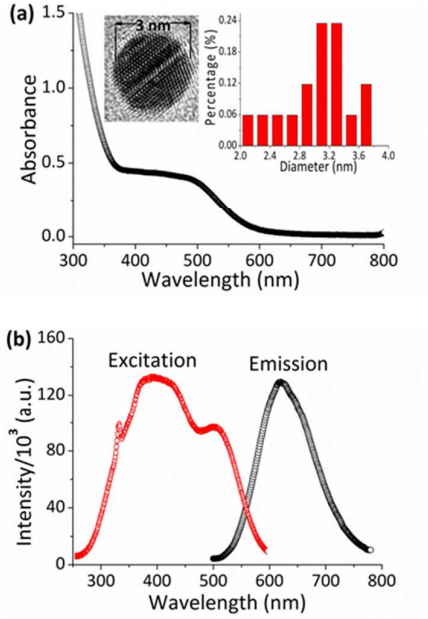

Fig.1. (a) UV–Vis absorption spectra of Ag@SG NCs. Insets: The left is an amplified TEM image of a silver nanocluster. The right is the size of diameter distribution of a typical Ag NCs sample. (b) Fluorescence excitation and emission spectra of Ag@SG NCs.

Following the successful synthesis of Ag@SG NCs, we have performed a study of ions detection by observing the fluorescence changes of NCs when dropping aqueous metal ions. As shown in **Fig. 2a**, the obtained Ag@SG NCs display strong fluorescence emission at ~630 nm, however, the fluorescence emission intensities change at the presence of different cationic metal ions. The cationic ions Fe^{3+}, Co^{2+}, Cd^{2+}, Ca^{2+}, Cr^{3+}, Cu^{2+}, Pb^{2+}, Ni^{2+} and Zn^{2+} were found to enhance the nascent fluorescence intensity of NCs to different extents; however, the addition of Mn^{2+} to Ag@SG NCs exclusively result in a remarkable fluorescence quenching.

To further expound the selectivity of Ag@SG NCs for Mn^{2+}, we have conducted a competitive experiment endeavouring to evaluate the practical effect in detecting Mn^{2+} ions at the presence of other metal ions. As shown in **Fig. 2b**, the coexistence of 0.1 equivalent of other metal ions in 1.0 mM Mn^{2+} ions also lead to obvious fluorescence quenching effect. Therefore it is credible for the use of Ag NCs to detect Mn^{2+} ions up to millimoles even in the presence of other interference metal cations (up to 0.1 mM in this study), revealing that Ag@SG NCs bear high selectivity toward Mn^{2+} among the metal ions in water.

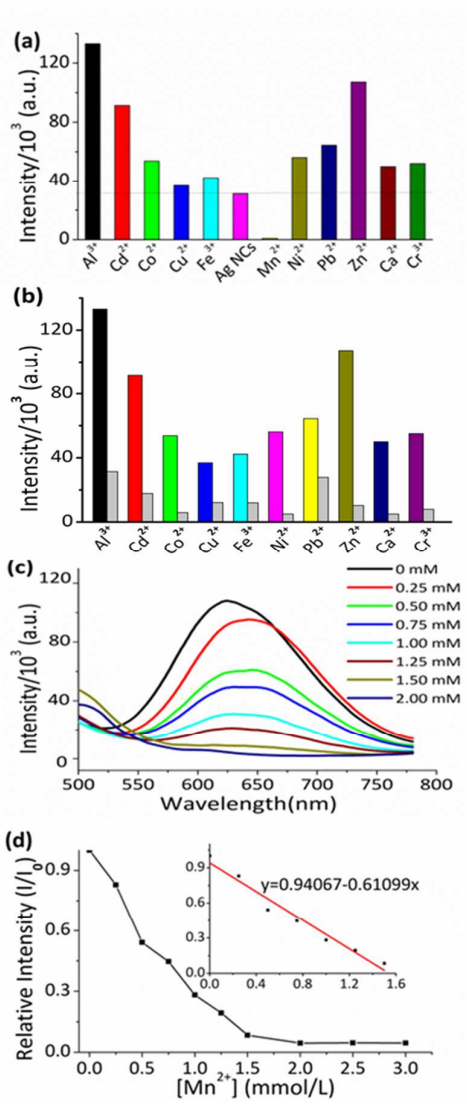

Fig.2. (a) Fluorescence responses of Ag@SG NCs (2.5 μg/mL) in H_2O to metal cations (0.1 mM). (b) Fluorescence intensity of Ag@SG NCs (2.5 μg/mL) with Mn^{2+} (1.0 mM) in the presence of various metal ions (0.1 mM) at 630 nm. Red bars: Ag@SG NCs with metal ions stated. Black bars: solutions of Ag@SG NCs with Mn^{2+} and 0.1 equivalent of the other ions stated. (c) Fluorescence titration profiles (λ_{ex} = 400 nm) of Ag@SG NCs (10 μg/mL) in the presence of increasing amounts of Mn^{2+} in H_2O. (d) The relative intensity (I/I_0) of Ag@SG NCs with the Mn^{2+} increasing monitored at 630nm with λ_{ex}= 400 nm. Inset: the linear detection range for 0-1.5 mM of Mn^{2+}.

We have also conducted fluorescence titration experiments for the silver NCs when adding Mn^{2+} ions of varying concentrations (**Fig. 2c)**. The fluorescence intensity at 630 nm decreases remarkably with increasing concentrations of Mn^{2+} ions. Upon further increase of the Mn^{2+} concentration, fluorescence emission tends to be quenched completely. Further analysis depicted in **Fig. 2d** reveals that there is a good linear relationship (coefficient of determination R^2=0.97) in the low concentration range of 0 to 1.5 mM although a

linear convergence beyond 2.0 mM. From the linear fitting curve (red) it is deduced that the limit of detection for Mn^{2+} ions is ~9.2 μM indicating decent sensitivity of this method which is comparable to the other reported chemosensors for detecting Mn^{2+} ions.[44-47]

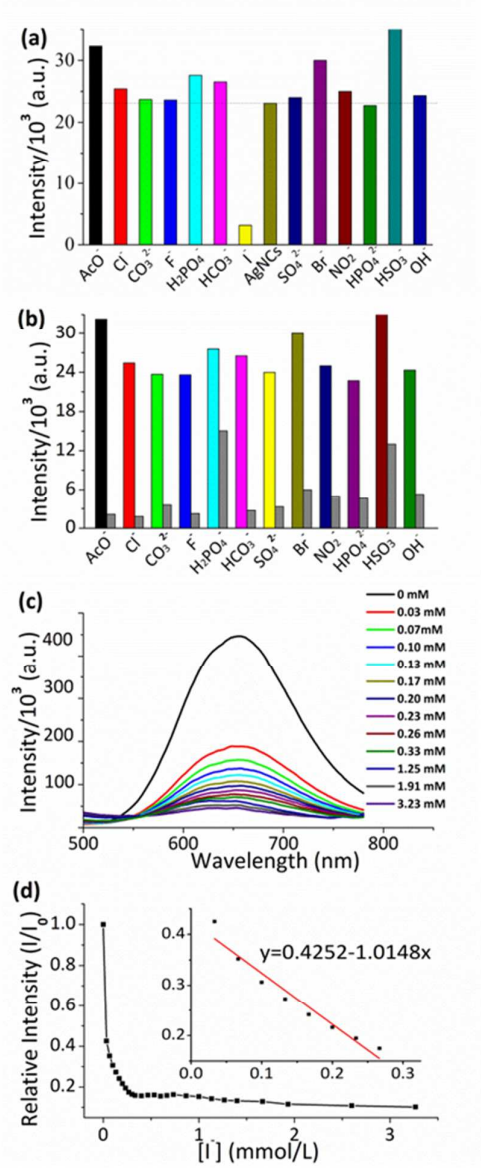

Fig.3. (a) Fluorescence response of Ag@SG NCs (2.5 μg/mL) in H_2O with anions (0.1 mM). (b) Fluorescence intensity of Ag@SG NCs (2.5 μg/mL) with I^- (0.1mM) in the presence of various anions (0.1 mM) at 630 nm. Red bars: Ag@SG NCs with anions stated. Black bars: solutions of Ag@SG NCs with I^- and 1.0 equivalent of the other anions stated. (c) Fluorescence titration profiles (λ_{ex} = 400 nm) of Ag@SG NCs (2.5 μg/mL) in the presence of increasing amounts of I^-. (d) The relative intensity (I/I_0) of Ag@SG NCs (2.5 μg/mL) with I^- concentration increasing at 630nm, λ_{ex} = 400 nm. Inset: the linear detection range for 0.03–0.26 mM of I^-.

Interesting results were noted when we further examined the selectivity of the Ag@SG NCs toward anions. **Fig. 3a** displays the fluorescence responses in water with F^-, Cl^-, Br^-, I^-, NO_2^-, CO_3^{2-}, AcO^-, $H_2PO_4^-$, HCO_3^-, SO_4^{2-}, HPO_4^{2-}, HSO_3^-, and OH^- among which only I^- quenches the fluorescence of Ag@SG NCs while the other anions even bring minor enhancements to their fluorescence intensities. Similar to the aforementioned case for Mn^{2+}, we have also performed competition experiments for I^- at the presence of the other anions, as shown in **Fig. 3b**. It is notable that the presence of other anions had no obvious interference comparing with the experimental results when only adding I^- itself. In the fluorescence titration experiment of Ag@SG NCs with I^- (**Fig. 3c)**, the fluorescence intensity decreased with increasing I^- concentrations, plotting out a good linear relationship (R^2=0.96) in the concentration range from 0.03 mM to 0.26 mM. The limit of detection for I^- was calculated to be ~5.9 μM (**Fig. 3d**), indicating good sensitivity to the detection of I^- ions, which is comparable to the previously published reports.[40, 41] It is additionally worth mentioning that, when S^{2-} ions exist in the solution, Ag@SG NCs do not show good selectivity for I^- ions, which is probably caused by the strong affinity of silver toward S^{2-} ions.[2]

3.2 The differentiation of Mn^{2+} and I^-

To further validate the high selectivity of Ag@SG NCs as a chemosensor for the detection of Mn^{2+} and I^- in practice, the fluorescence responses of Ag@SG NCs at the presence of Mn^{2+} upon the addition of a number of anions (F^-, Cl^-, Br^-, I^-, NO_2^-, CO_3^{2-}, AcO^-, $H_2PO_4^-$, HCO_3^- SO_4^{2-}, HPO_4^{2-}, HSO_3^-, and OH^-) were examined. Also examined is the responses of "Ag@SG NCs + I^-" when adding metal ions (Fe^{3+}, Co^{2+}, Cd^{2+}, Ca^{2+}, Cr^{3+}, Cu^{2+}, Pb^{2+}, Ni^{2+} and Zn^{2+}). As shown in **Fig.4a** and **4b**, the coexistence of 1.0 equivalent of other metal ions and anions did not interfere with the Mn^{2+} and I^- quenching effects. Besides, when Mn^{2+} and I^- ions were added into Ag@SG NCs simultaneously, the fluorescence was also quenched. So, whether or not to be able to distinguish cationic Mn^{2+} from anion I^-?

With this in mind, we have studied the ratiometric absorption behaviors for Mn^{2+} and I^-, respectively. **Fig. 5** presents UV-Vis titration experiments of Ag@SG NCs in the presence of increasing concentrations of Mn^{2+} and I^- ions, respectively. It is notable that the position of the broad absorption band from 350 nm to 500 nm displays rare changes, but the intensity decreased gradually with the Mn^{2+} ions increasing (**Fig. 5a**). This result excludes the possibility of direct binding of Mn^{2+} to the Ag atoms due to that the absorption band of Ag nanoclusters is very sensitive to the presence of adsorbed substances. [48] However, the gradual addition of I^- ions (**Fig. 5b** and **5c**) differs distinctly from that of Mn^{2+}. Besides the gradual decrease of the wide absorption band from 400 nm to 500 nm, two iso-absorptive points are noted successively in different concentration ranges. The first isobestic point emerges at ~398 nm with I^- concentration increasing in the lower concentration range, while more gradual addition of I^- ions leads to the second iso-absorptive point at ~378 nm. In addition, the spectrum exhibits a new absorption peak at ~420 nm in the higher I^- concentration range. Exclusion experiments were conducted by observing UV-Vis absorption spectra of HSG aqueous at the presence of I^- ions (**Fig. S5, ESI**), however, the addition of I^- to HSG solution was found to

bring negligible changes. Therefore, the likely formed new complexes in the solution come to be associated with the reaction of Ag@SG NCs core and I^- ions. These results indicated that Ag@SG NCs could be used to distinguish Mn^{2+} from I^- by the ratiometric absorption spectrometry method.

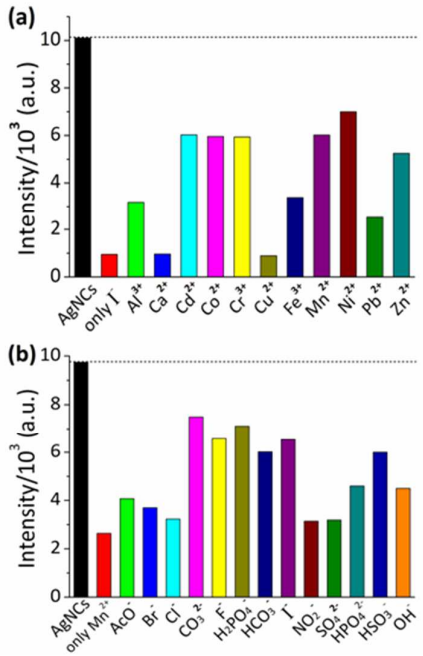

Fig.4. Fluorescence spectra of **(a)** Ag NCS + I^- upon the addition of metal ions, **(b)** Ag NCS + Mn^{2+} upon the addition of anions in H_2O.

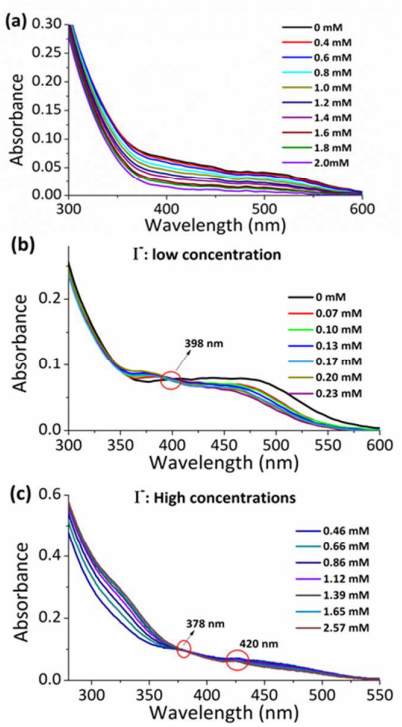

Fig.5. UV-Vis titration spectra of Ag@SG NCs (10 μg/mL) in the presence of increasing amounts of Mn^{2+} **(a)** and Ag@SG NCs (2.5 μg/mL) in the presence of increasing amounts of I^- **(b/c)**.

3.3 The sensing mechanisms

The above experimental results demonstrate an interesting fact that the as-prepared Ag@SG NCs are highly sensitive for detecting and differentiating Mn^{2+} and I^- ions. Such a chemosensor that plays both ends against ions detection is rarely obtained in previously reported studies. In order to provide insights into the sensing mechanism, ^{1}H NMR experiments and TEM characterizations of Ag@SG NCs before and after the addition of Mn^{2+} and I^- have been conducted. As shown in **Fig. 6A**, upon the gradual addition of Mn^{2+} to Ag@SG NCs, all proton signals of Ag@SG NCs disappear until finally only a solvent D_2O peak existing at 4.79 ppm. With Mn^{2+} ions concentration further increasing, there was brown precipitate out of the solution. While in the case of I^- (**Fig. 6B**), all proton signals are almost the same indicating that the chemical environment of all the protons of –SG do not encounter obvious changes. By TEM photographic observation, the nascent Ag@SG NCs display monodispersity (**Fig. S2a** and **b, ESI**); however, there is aggregation pattern at the presence of Mn^{2+} **(Fig. S2c** and **d, ESI)**; in contrast, while adding I^- ions **(Fig. S2e** and **f, ESI)** the average size of particles becomes apparently larger than the original Ag@SG NCs. A pending question is that what determines the differences for Mn^{2+} and I^- ions rendering fluorescence quenching of Ag NCs?

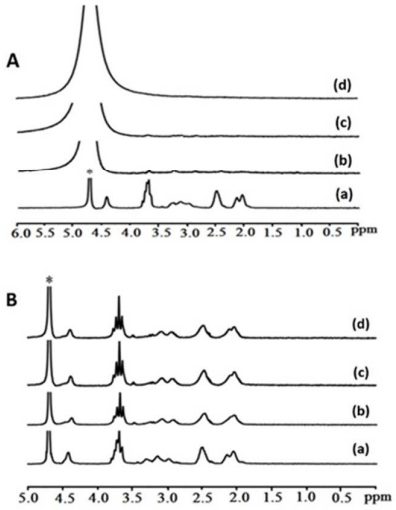

Fig.6. ^{1}H NMR spectra in D_2O: (A) Ag@SG NCs at ~10 μg/mL (a), after adding 0.5 mM of Mn^{2+} (b), 1.0 mM of Mn^{2+} (c), and 2.0 mM of Mn^{2+} (d). (B) Ag@SG NCs at ~2.5 μg/mL(a), and that after adding 0.03 mM of I^-(b), 0.1 mM of I^- (c), and 0.3 mM of I^-(d). The D_2O peak at 4.79 ppm is labelled with *.

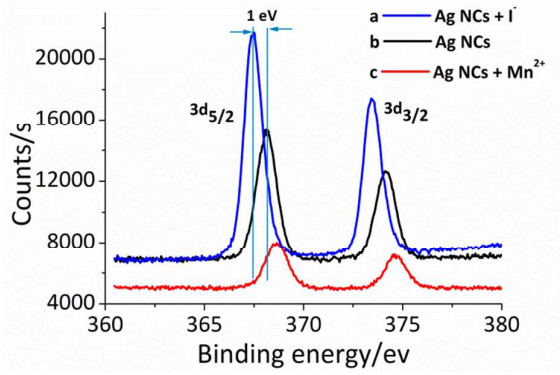

Fig. 7. XPS spectra of Ag 3d core-level for the Ag@SG NCs at the absence (a) and presence of I^- (b) and Mn^{2+} (c) ions.

Fig. 7 provides a comparison of XPS patterns of Ag 3d core-level for the Ag@SG NCs before and after reacting with Mn^{2+} and I^- ions. For the case when adding I^- ions (**Fig. 7b**), it is clearly noted that both the peaks assigned to Ag-$3d_{5/2}$ (368.2 eV) and Ag-$3d_{3/2}$ (374.1 eV) shift to the lower-energy side up to 1.0 eV in the presence of I^- ions. This is in sharp contrast to the situation when adding Mn^{2+} ions where the minor shift is towards high-energy region (**Fig. 7c**). The low-energy shifts at the presence of iodide ions demonstrate the complexation of Ag with electron-rich groups or elements such as iodide. This is an important piece of evidence as fluorescence quenching often could be caused by energy transfer or static quenching by forming nonfluorescent complexes. Actually many studies about the interactions of halide ions with silver or other nanoparticles have been reported,[49-51] and it is known that iodides have a stronger affinity for noble metal nanoclusters than the other counterparts.[52-54] Further evidences are determined by noting the presence of Ag_nI_x species *via* mass spectrometry (**Fig. S6, ESI**). Combining with the ratiometric absorption behaviors for I^- (**Fig. 5b, 5c**), the isobestic points indicate that there are multiple reaction pathways in the solution of Ag@SG NCs with gradual addition of I^-. It is ascertained that I^- ions in low concentration absorb on the Ag@SG NCs surface rapidly owing to their high affinity of Ag-I bond or the low solubility of AgI, which leads to the catalysed etching likely *via* a reaction pathway analogous to that of strong acid swapping out weak acid, as described in **Equation 1**:

$$Ag_n(SG)_x^- + y\,I^- + y\,H^+ \rightarrow Ag_{n-y}(AgI)_y(SG)_{x-y}^- + y\,HSG, \quad \text{or}$$

$$Ag_n(SG)_x^- + y\,I^- + y\,H^+ + y\,H_2O \rightarrow Ag_{n-y}(SG)_{x-y}^- + y\,AgI(H_2O)^0 + y\,HSG \quad (1)$$

In this equation, the formation of $Ag_{n-y}(AgI)_y(SG)_{x-y}^-$ or $AgI(H_2O)^0$ species adsorbed in the Stern plane of Ag@SG NCs may play a role in the stability by truncating the van der Waals attraction at distances of closest approach relative to the electrostatic repulsion interactions.[55] Next, more I^- ions chemisorbed on the surface of nanocluster may rearrange the surface charges,[1] which will increase the weak intermolecular interactions among the newly formed iodide-interspersed silver particles and then lead to aggregation. At the same time, a small number of protection ligands means reduced sizes of the NCs, allowing for increased specific surface area and free surface energy hence incidental aggregation **(Equation 2)**.

$$Ag_{n-y}(AgI)_y(SG)_{x-y}^- + Ag_n(SG)_x^- + z\,I^- + \gamma\,H^+ \rightarrow Ag_{2n}I_{y+z}(SG)_\delta(HSG)_\gamma^-, \text{ or}$$

$$Ag_n(SG)_x^- + y\,AgI(H_2O)^0 + y\,I^- \rightarrow Ag_{n+y}I_{2y}(SG)_{x-y}(HSG)_y^- + y\,OH^-, \text{ or}$$

$$Ag_{n-y}(SG)_y^- + Ag_{n-y}(SG)_y^- + z\,I^- + \gamma\,H^+ \rightarrow Ag_{2n-2y}I_z(SG)_\delta(HSG)_\gamma^- \quad (2)$$

Where the values of x, y, z and n are integer (i.e., 0 to n). In brief, within the chemosensor mechanism, I^- ions interact with Ag@SG initially *via* an etching-like pathway prevailing in low I^- concentrations, while aggregation/reorganization dominates in the high concentrations of I^- ions. Considering that the chemosensing mechanism for I^- ions could be pH-dependent, these equations indicate the tendency to form a class of $Ag_xI_y(SG)_z(HSG)_r^-$ complexes, which are actually in accordance with previous proposals.[40, 41] It is worth mentioning that the characteristic surface plasmon resonance (SPR) band of Ag nanoparticles locating around 420 nm [1] was found in the higher I^- concentration range in **Fig. 5c**, which was also in accordance with the average size as typically displayed in a TEM image **(Fig. S2f, ESI)**.

Different from I^- ions, the result that Mn^{2+} induces aggregation of Ag@SG NCs in solution could simply follow a well-known AIFQ (Aggregation Induced Fluorescence Quenching) mechanism, which profits from the interaction of hard acid Mn^{2+} ions with the multiple hard base –NH and -O atoms presenting in several –SG ions. What's more, Mn^{2+} is a highly paramagnetic element, which benefits to quench the fluorescence of metal NCs *via* energy transfer and weak bondings (**Equation 3**).

$$Ag_n(SG)_x^- + Ag_m(SG)_y^- + Mn^{2+} \rightarrow \left[Ag_n(GS)_x \cdots Mn \cdots (SG)_yAg_m\right]^0 \quad (3)$$

3.4 Cell toxicity and bioimaging

Having depicted the excellent selectivity and high sensitivity of Ag@SG NCs towards Mn^{2+} and I^- ions in water, we are endeavouring to explore its potential application in living cell bioimaging. It is well known that a small quantity of Mn^{2+} is necessary for living organism, such as bearing influences to bone growth, also glucose and fat metabolism as well as the use for antioxidant and prevention from cancer and anemia, etc. While excessive intakes bring in toxic symptoms and neurodegenerative disorders.[56] Iodine, also plays an important role in biological activities due to its being required for the normal function of thyroid and neurologic activity.[5-8] Deficiency of iodine causes health problems such as cretinism, congenital abnormalities and goiter;[5-8] however, excessive amount of iodine in human body may give rise to thyrotoxicosis.[8, 9] Therefore, we have firstly tested the toxicity of the as-prepared silver NCs to MCF-7 cells (**Fig. 8a**). The cellular toxicity of Ag@SG NCs to MCF-7 cells in H_2O was determined by a MTT assay with the concentration of Ag@SG NCs ranged from 0 to 0.5μg/mL (**Fig. 8b**). Upon incubation for 24 h of 0.25 μg/mL Ag@SG NCs (a normal concentration used for confocal imaging studies), the cellular viabilities are estimated nearly 100%, revealing that the as-

prepared Ag@SG NCs are almost not toxic for MCF-7 cells. The reason of hypotoxicity is largely ascribed to the eco-friendly stabilization ligand GSH and proper PH values that we have maintained in synthesizing the Ag@SG NCs.

The final important result is the attempt to detect Mn^{2+} and I^- in living cells. For this study, the MCF-7 cells were incubated with 0.25 μg/mL Ag@SG NCs for 2 h firstly, and then treated with 1.5 mM Mn^{2+} and 0.3 mM I^- for 30 min, respectively. As shown in **Fig. 9a**, the cells only incubated with Ag@SG NCs display strong fluorescence, while the strong red fluorescence quenches in cells when exposed to aqueous solution of Mn^{2+} (**Fig. 9b**) and I^- (**Fig. 9c**) ions. It is noted that the chemosensor of Ag@SG NCs behaves cell-permeable allowing for bioimaging in living cells and the decent fluorescence on/off property enables to detect intracellular Mn^{2+} and I^- ions. Besides, the shape of the MCF-7 cells further indicated no cytotoxicity effect of the Ag@SG NCs and no aggregation on the membrane. Our biolabeling and chemosensing effect in living cells is comparable to the recent reports in this field, such as GSH-protected silver nanoclusters used in A549 cells imaging by Le Guevel et al.,[57] and the Ag NCs were used to demonstrate cytocompatible and show better inhibition effects through MTT assay by Li et al.[58]

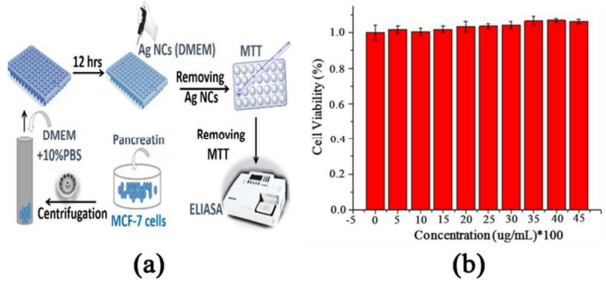

Fig.8. (a) The general operation process. MTT: methyl thiazolyl tetrazolium; DMEM: Dulbecco's Modified Eagle Medium. (b) Cell viability values estimated by MTT proliferation test versus concentrations of Ag@SG NCs after 24 h incubation at 37°C.

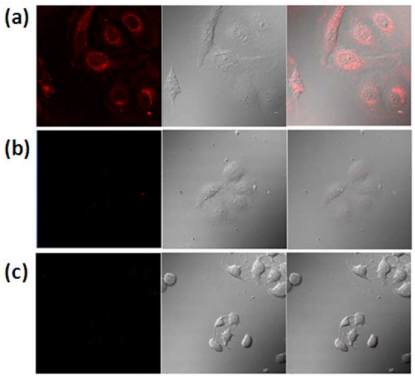

Fig.9. Confocal fluorescence images of (a) only Ag@SG NCs, (b) addition of Mn^{2+} and (c) addition of I^- in MCF-7 cells in the fluorescence (left), Bright (middle), and overlay (right) field.

4. Conclusions

In summary, we develop here an eco-friendly chemosensor — glutathione-protected silver nanoclusters, synthesized *via* a simple and green route. Utilizing this Ag@SG NCs chemosensor, we have attained the detection and differentiation of Mn^{2+} and I^- ions with high selectivity and sensitivity. The sensing mechanisms are deduced according to the fluorescence and UV-Vis titration, ^1H NMR, TEM images, XPS analyses etc. For the detection of Mn^{2+} ions, the silver NCs are prone to aggregate *via* $[Ag_n(GS)_x \cdots Mn \cdots (SG)_yAg_m]^0$, leading to the fluorescence quenching. In comparison, the detection for I^- ions was based on the large affinity of silver halides resulting in iodide-induced etching and aggregation/reorganization. We have successfully applied the chemosensor Ag@SG NCs to detect intracellular Mn^{2+} and I^- ions, which would broaden the applications of functionalized Ag NCs in biological fields.

Acknowledgments

This work is supported by the Young Professionals Programme in Institute of Chemistry, Chinese Academy of Sciences (ICCAS-Y3297B1261).We thank the financial support from CAS of China with Grant No. Y31M0112C1.

Notes and References

1 F. Qu, N. B. Li and H. Q. Luo, Anal. Chem., 2012, 84, 10373-10379.
2 M. Wang, Z. Wu, J. Yang, G. Wang, H. Wang and W. Cai, Nanoscale, 2012, 4, 4087-4090.
3 R. Li, P. Xu, J. Fan, J. Di, Y. Tu and J. Yan, Anal. Chim. Acta, 2014, 827, 80-85.
4 A. P. de Silva, H. Q. N. Gunaratne, T. Gunnlaugsson, A. J. M. Huxley, C. P. McCoy, J. T. Rademacher and T. E. Rice, Chem. Rev., 1997, 97, 1515-1566.
5 R. H. Verheesen and C. M. Schweitzer, Medical Hypotheses, 2008, 71, 645-648.
6 M. Haldimann, B. Zimmerli, C. Als and H. Gerber, Clinical Chemistry, 1998, 44, 817-824.
7 F. Jalali, M. J. Rajabi, G. Bahrami and M. Shamsipur, Anal. Sci., 2005, 21, 1533-1535.
8 R. P. Li, P. P. Xu, J. Fan, J. W. Di, Y. F. Tu and J. L. Yan, Anal. Chim. Acta, 2014, 827, 80-85.
9 R. Hu, L. Zhang and H. B. Li, New J. Chem., 2014, 38, 2237-2240.
10 A. W. Castleman, Jr. and S. N. Khanna, J. Phys. Chem. C, 2009, 113, 2664-2675.
11 Z. Luo, G. U. Gamboa, J. C. Smith, A. C. Reber, J. U. Reveles, S. N. Khanna and A. W. Castleman, Jr., J. Am. Chem. Soc., 2012, 134, 18973-18978.
12 Z. Luo, C. J. Grover, A. C. Reber, S. N. Khanna and A. W. Castleman, J. Am. Chem. Soc., 2013, 135, 4307-4313.
13 Z. Luo and A. W. Castleman, Jr., Acc. Chem. Res., 2014, 2931-2940.
14 L. A. Peyser, A. E. Vinson, A. P. Bartko and R. M. Dickson, Science, 2001, 291, 103-106.
15 J. Zheng and R. M. Dickson, J. Am. Chem. Soc., 2002, 124, 13982-13983.
16 S. W. Chen, R. S. Ingram, M. J. Hostetler, J. J. Pietron, R. W. Murray, T. G. Schaaff, J. T. Khoury, M. M. Alvarez and R. L. Whetten, Science, 1998, 280, 2098-2101.
17 Y. Y. Yang and S. W. Chen, Nano Lett., 2003, 3, 75-79.
18 Y. Cui, Y. Wang, R. Liu, Z. Sun, Y. Wei, Y. Zhao and X. Gao, ACS Nano, 2011, 5, 8684-8689.
19 H. Xu and K. S. Suslick, ACS Nano, 2010, 4, 3209-3214.

20 J. P. Wilcoxon and B. L. Abrams, Chem. Soc. Rev., 2006, 35, 1162-1194.
21. X. Liu, Y. Wu, S. Li, Y. Zhao, C. Yuan, M. Jia, Z. Luo, H. Fu and J. Yao, Rsc Adv., 2015, 5, 30610-30616.
22 L. Shang, S. J. Dong and G. U. Nienhaus, Nano Today, 2011, 6, 401-418.
23 Y. Wang, Y. Cui, R. Liu, Y. Wei, X. Jiang, H. Zhu, L. Gao, Y. Zhao, Z. Chai and X. Gao, Chem. Commun., 2013, 49, 10724-10726.
24 Y. Wang, Y. Cui, Y. Zhao, R. Liu, Z. Sun, W. Li and X. Gao, Chem. Commun., 2012, 48, 871-873.
25 R. Liu, J. Zhai, L. Liu, Y. Wang, Y. Wei, X. Jiang, L. Gao, H. Zhu, Y. Zhao, Z. Chai and X. Gao, Chem. Commun., 2014, 50, 3560-3563.
26 W. Li, R. Liu, Y. Wang, Y. Zhao and X. Gao, Small, 2013, 9, 1585-1594.
27 Y. M. Guo, Z. Wang, H. W. Shao and X. Y. Jiang, Analyst, 2012, 137, 301-304.
28 J. P. Xie, Y. G. Zheng and J. Y. Ying, Chem. Commun., 2010, 46, 961-963.
29 D. Y. Cao, J. Fan, J. R. Qiu, Y. F. Tu and J. L. Yan, Biosens. Bioelectron., 2013, 42, 47-50.
30 Y. L. Liu, K. L. Ai, X. L. Cheng, L. H. Huo and L. H. Lu, Adv. Funct. Mater., 2010, 20, 951-956.
31 X. X. Wang, P. Wu, X. D. Hou and Y. Lv, Analyst, 2013, 138, 229-233.
32 E. S. Shibu, M. A. H. Muhammed, T. Tsukuda and T. Pradeep, J. Phys. Chem. C, 2008, 112, 12168-12176.
33 A. Baksi, M. S. Bootharaju, X. Chen, H. Häkkinen and T. Pradeep, J. Phys. Chem. C, 2014, 118, 21722-21729.
34 Z. Wu, M. Wang, J. Yang, X. Zheng, W. Cai, G. Meng, H. Qian, H. Wang and R. Jin, Small, 2012, 8, 2028-2035.
35 Z. Chen, D. Lu, G. Zhang, J. Yang, C. Dong and S. Shuang, Sensor Actuat B-Chem., 2014, 202, 631-637.
36 C. L. Zheng, Z. X. Ji, J. Zhang and S. N. Ding, Analyst, 2014, 139, 3476-3480.
37 W.-H. Ding, C. Wei, X.-J. Zheng, D.-C. Fang, W.-T. Wong and L.-P. Jin, Inorg. Chem., 2013, 52, 7320-7322.
38 W.-H. Ding, D. Wang, X.-J. Zheng, W.-J. Ding, J.-Q. Zheng, W.-H. Mu, W. Cao and L.-P. Jin, Sensor Actuat B-Chem., 2015, 209, 359-367.
39 W.-H. Ding, W. Cao, X.-J. Zheng, W.-J. Ding, J.-P. Qiao and L.-P. Jin, Dalton Trans., 2014, 43, 6429-6435.
40 A. Kumar, R. K. Chhatra and P. S. Pandey, Org. Lett., 2010, 12, 24-27.
41 J. Zhang, X. Xu, C. Yang, F. Yang and X. Yang, Anal. Chem., 2011, 83, 3911-3917.
42 A. Baksi, M. S. Bootharaju, X. Chen, H. Hakkinen and T. Pradeep, J. Phys. Chem. C, 2014, 118, 21722-21729.
43 G. Gonella, O. Cavalleri, S. Terreni, D. Cvetko, L. Floreano, A. Morgante, M. Canepa and R. Rolandi, Surf. Sci., 2004, 566, 638-643.
44 P. S. Hariharan and S. P. Anthony, Spectrochim Acta a, 2015, 136, 1658-1665.
45 K. B. Kim, G. J. Park, H. Kim, E. J. Song, J. M. Bae and C. Kim, Inorg. Chem. Commun., 2014, 46, 237-240.
46 C. Gou, H. Wu, S. Jiang, C. Yi, J. Luo and X. Liu, Chem. Lett., 2011, 40, 1082-1084.
47 I. Kaya, M. Yildirim and M. Kamaci, Synth. Met., 2011, 161, 2036-2040.
48 T. Linnert, P. Mulvaney and A. Henglein, J. Phys. Chem., 1993, 97, 679-682.
49 J. Zhang, X. Xu, C. Yang, F. Yang and X. Yang, Anal. Chem., 2011, 83, 3911-3917.
50 J. Zhang, Y. Yuan, X. Xu, X. Wang and X. Yang, ACS Appl. Mater. Interfaces, 2011, 3, 4092-4100.
51 M. G. Espinoza, M. L. Hinks, A. M. Mendoza, D. P. Pullman and K. I. Peterson, J. Phys. Chem. C, 2012, 116, 8305-8313.
52 O. M. Magnussen, Chem. Rev., 2002, 102, 679-725.
53 J. E. Millstone, W. Wei, M. R. Jones, H. Yoo and C. A. Mirkin, Nano Lett., 2008, 8, 2526-2529.
54 M. Zhu, G. Chan, H. Qian and R. Jin, Nanoscale, 2011, 3, 1703-1707.
55 Z. Luo, J. C. Smith, T. M. Goff, J. H. Adair and A. W. Castleman, Jr., Chem. Phys., 2013, 423, 73-75.
56 B. A. Pappas, D. Zhang, C. M. Davidson, T. Crowder, G. A. S. Park and T. Fortin, Neurotoxicol. Teratol., 1997, 19, 17-25.
57 X. Le Guevel, C. Spies, N. Daum, G. Jung and M. Schneider, Nano Res., 2012, 5, 379-387.
58 J. Li, X. Zhong, F. Cheng, J.-R. Zhang, L.-P. Jiang and J.-J. Zhu, Anal. Chem., 2012, 84, 4140-4146.